Journal of Alloys and Compounds 509 (2011) 5688–5691

Contents lists available at ScienceDirect

Journal of Alloys and Compounds

journal homepage: www.elsevier.com/locate/jallcom

Structure and electrical conduction behavior of $LiZnVO_4$ ceramic prepared by solution-based chemical route

Moti Ram*

Department of Physics and Meteorology, Indian Institute of Technology, Kharagpur, West Bengal 721302, India

ARTICLE INFO

Article history:
Received 17 November 2010
Received in revised form 20 February 2011
Accepted 22 February 2011
Available online 1 March 2011

Keywords:
Ceramics
Chemical method
X-ray diffraction
Complex electrical impedance
Electrical conductivity

ABSTRACT

In the present work, an evaluation of the structural and electrical properties of a compound ($LiZnVO_4$) has been undertaken. This compound was prepared by solution-based chemical route. The electrical properties were measured using a.c. impedance spectroscopy method in the frequency range of 10^3–10^6 Hz at various temperatures from 28 to 300 °C. X-ray diffraction study indicates a rhombohedral unit cell structure with lattice parameters $a = 14.1934$ Å, $b = 14.1934$ Å, $c = 9.4926$ Å, $V = 1656.12$ (Å)^3, $\alpha = 90°$, $\beta = 90°$ and $\gamma = 120°$. A field emission scanning electron micrograph reveals a polycrystalline texture of the compound with grains of unequal sizes ~0.2–2.0 μm. The electrical conduction in the material is a thermally activated process due to the bulk effect. Frequency dependence of a.c. conductivity obeys Jonscher's universal law ($\sigma_{ac} = \sigma_{dc} + A\omega^n$).

1. Introduction

Lithium-containing transition metal oxides have continued to attract attention over the years [1–9]. They have a large non-stoichiometry and high-valence state of transition metal ions, which affect the physical (electrical, magnetic, dielectric, etc.) properties to provide useful information [5]. Furthermore, the physical properties of these oxides are controlled by the preparation conditions, chemical composition, sintering temperature and time, type and amount of substitutions. Electrical measurements have been considered as an important tool for studying the electrical transport properties of these materials [6,10–15]. The a.c. impedance spectroscopy is a very convenient and powerful experimental technique for electrical measurements. This technique enables us to correlate the electrical properties of a material with its microstructure, and also helps to analyze and separate the contributions from various components (i.e., grains, grain boundary, interfaces, etc.) of polycrystalline materials in the wide frequency range [10–15]. From the measured data, the complex impedance function is computed as $Z^* = Z' - jZ''$, where Z' and Z'' are the real and imaginary parts of Z^* respectively, and $j = (-1)^{1/2}$. The complex impedance diagrams helps to build up an equivalent circuit model for the conduction process of charged carriers [10–15]. Many researchers have used a.c. impedance spectroscopy technique to characterize the electrical transport properties of lithium-containing transition metal oxides [6,16–22]. In the present work, I have studied the structural and electrical properties of a lithium-containing transition metal oxide ($LiZnVO_4$), which is prepared by solution-based chemical route. The electrical properties of this oxide are studied using an a.c. impedance spectroscopy technique. Crystal structure is examined by X-ray diffraction method.

2. Experimental procedures

2.1. Material preparation

A solution-based chemical route was used to synthesize the $LiZnVO_4$ fine powder. The stoichiometric amounts of highly pure $LiNO_3$, $Zn(NO_3)_2{\cdot}6H_2O$ and NH_4VO_3 were dissolved in distilled water and mixed together. Thereafter triethanolamine was added maintaining a ratio of 3:1 with metal ions. HNO_3 and oxalic acid were added to dissolve the precipitate and then the clear solution was evaporated at temperature (~200 °C) with continuous stirring. A fluffy, mesoporous and carbon-rich precursor mass was formed by complete evaporation of the solution. After grinding, the voluminous, fluffy and black carbonaceous mass was calcined at 550 °C for 2 h to produce a desired phase, which is confirmed by X-ray diffraction analysis. The calcined powder was cold pressed into circular disc shaped pellet of diameter 12–13 mm and various thicknesses with polyvinyl alcohol as a binder using hydraulic press at a load of ~3–4 tonnes. These pellets were then sintered at 575 °C for 1.5 h followed by slow cooling process. Subsequently, the pellets were polished by fine emery paper to make their faces smooth and parallel. The pellets were finally coated with conductive silver paint and dried at 150 °C for 3 h before carrying out electrical measurements.

2.2. Material characterization

Thermogravimetry (TG) and derivative thermogravimetry (DTG) of material powder (fluffy, mesoporous and carbon-rich precursor mass) was carried out using a simultaneous thermal analyzer (Perkin Elmer, Model: Pyris Diamond). X-ray diffraction of the calcined powder was studied at room temperature using a diffractometer

* Corresponding author. Tel.: +91 3222 281902.
E-mail address: motiram05@yahoo.co.in

0925-8388/$ – see front matter © 2011 Elsevier B.V. All rights reserved.
doi:10.1016/j.jallcom.2011.02.128

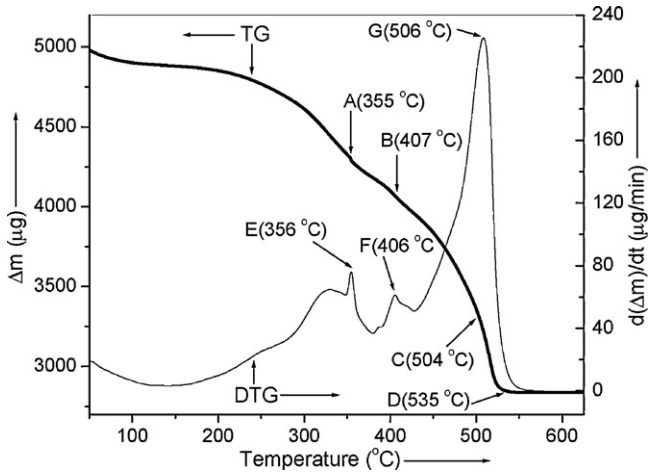

Fig. 1. TG and DTG curves of the precursor mass of $LiZnVO_4$.

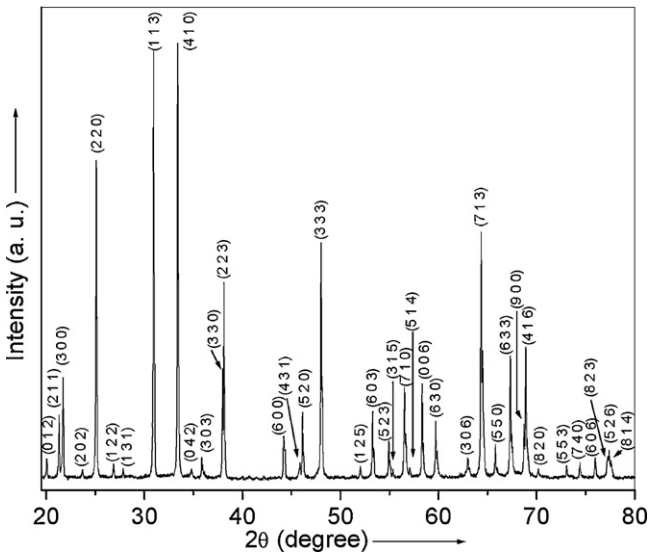

Fig. 2. X-ray diffraction pattern of $LiZnVO_4$ at room temperature.

(PANalytical PW 3040/60 X'Pert PRO) in the angle range $19^\circ \leq 2\theta \leq 80^\circ$ on being irradiated by Cu K_α radiation of wavelength equal to 1.5419 Å. The surface morphology of the gold-sputtered sample was recorded with different magnifications at room temperature using a ZEISS (Model: SUPRA™ 40) field emission scanning electron microscope. Electrical impedance, phase angle, tangent loss and capacitance were measured by applying a voltage of ~0.701 V using a computer-controlled frequency response analyzer (HIOKI LCR Hi TESTER, Model: 3532-50) with varying temperature over the frequency range of 10^3–10^6 Hz.

3. Results and discussion

Fig. 1 shows the TG and DTG curves of the material powder (fluffy, mesoporous and carbon-rich precursor mass). TG curve shows loss of mass on heating the material. The small depressions at points A (~355 °C), B (~407 °C) and C (~504 °C) may be attributed to mass loss due to the release of surface absorbed water present in the material, initiation of intermediate reaction steps among precursors and evolution of gases like CO_2 and NO_2, etc. towards the end of the reaction [23,24]. The mass loss appears to stop at the point D (~535 °C), which indicates the completion of reaction and formation of compound above point D. The observations of TG study are found to be in close agreement with DTG curve. DTG curve shows peaks at the points E (~356 °C), F (~406 °C) and G (~506 °C), which may be attributed to mass loss due to the release of surface absorbed water content, intermediate reaction steps and residual gas evolution towards the end of the reaction, when mass loss stagnates [23,24].

X-ray diffraction pattern of $LiZnVO_4$ at room temperature is given in Fig. 2, which confirms the formation of a single-phase compound. A standard software (POWD MULT) is used to index all peaks [25]. A rhombohedral unit cell structure is selected on the basis of good agreement between observed and calculated interplaner spacing (d-values). The least squares refined lattice parameters (as evaluated using the software) are $a = 14.1934$ Å, $b = 14.1934$ Å, $c = 9.4926$ Å, $V = 1656.12$ (Å)^3, $\alpha = 90^\circ$, $\beta = 90^\circ$ and $\gamma = 120^\circ$. These values are in good agreement with the JCPDS standard (Reference code: 38-1332).

Fig. 3 presents a field emission scanning electron micrograph at room temperature of material's sintered pellet. It is clear from the micrograph that the grains are densely packed in the sintered pellet and are granular in shape. This shape and distribution of grains in the microstructure exhibit the polycrystalline nature of the material. The grain size has been measured by linear intercept method [26] and it is in the range of ~0.2–2.0 μm. Furthermore, the grains of unequal sizes present an average grain size with polydisperse distribution on the surface of the ceramic.

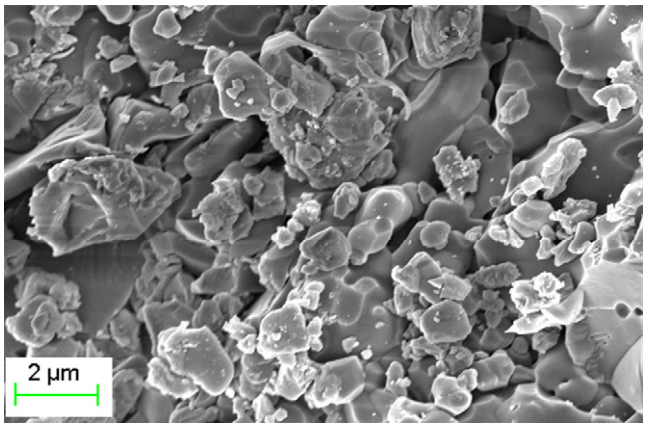

Fig. 3. Field emission scanning electron micrograph of $LiZnVO_4$ at room temperature.

The Nyquist plots [i.e., Z' versus Z'' graph) at different temperatures are given in Fig. 4. Depressed semicircles are observed in the pattern, which suggest the non-Debye type behavior of the material [10]. The presence of single depressed semicircle at studied temperatures indicates that electrical conduction in the material is due the bulk property of the material [10,27]. It is modeled by an equivalent electrical circuit (a parallel R–C circuit), which is given in Fig. 4 (inset). The intercept of the semicircle on the real axis gives the value of bulk resistance (R_b). The value of d.c. conductivity (σ_{dc}) has been calculated using the relation ($\sigma_{dc} = t/R_bA$), where t is the thickness of the sample and A is the effective area of the electrodes. The variation of $\log \sigma_{dc}$ with $10^3/T$ is given in Fig. 5. It is seen from Fig. 5 that the value of σ_{dc} increases with rise in temperature and follows an Arrhenius relation [$\sigma_{dc} = \sigma_o \exp(-E_a/kT)$], where σ_o is the pre-exponential factor corresponding to $1/T = 0$, E_a is the activation energy for charge transfer, k is the Boltzmann constant and T is the absolute temperature [28–32]. These features suggest about electrical conduction in the material as a thermally activated process. The value of E_a is calculated with the help of Arrhenius relation and slope of Fig. 5 as ~(0.078 ± 0.002 eV at 28–200 °C).

The frequency dependence of Z'' at different temperatures is presented in Fig. 6. It is observed that the values of Z'' decrease with rise in temperature and appear to merge at high frequency

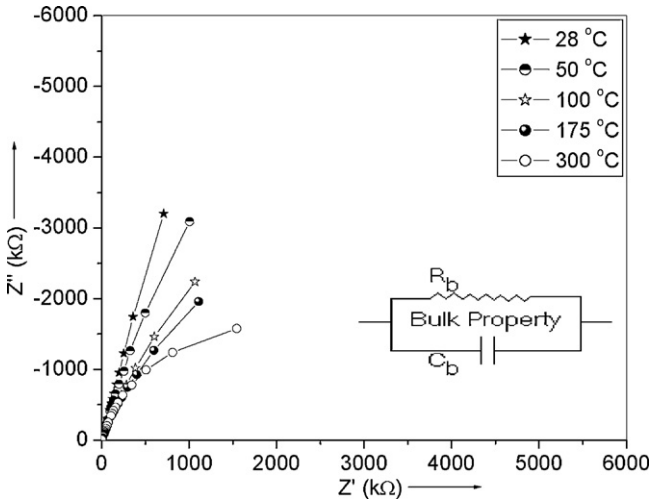

Fig. 4. Nyquist plots at different temperatures with electrical equivalent circuit (inset).

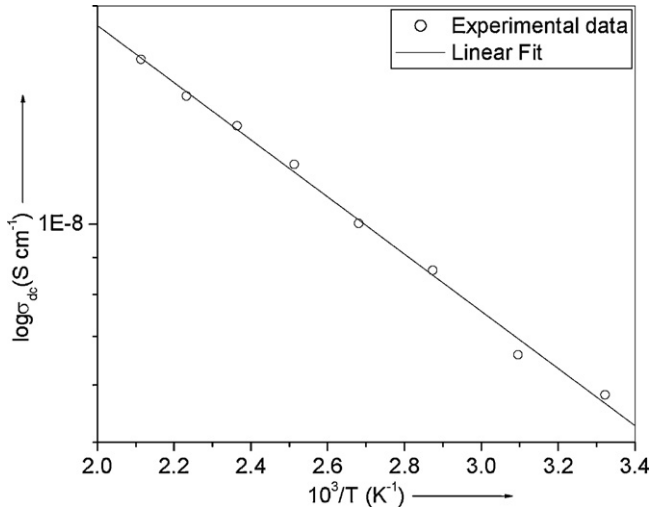

Fig. 5. Variation of σ_{dc} as a function of temperature.

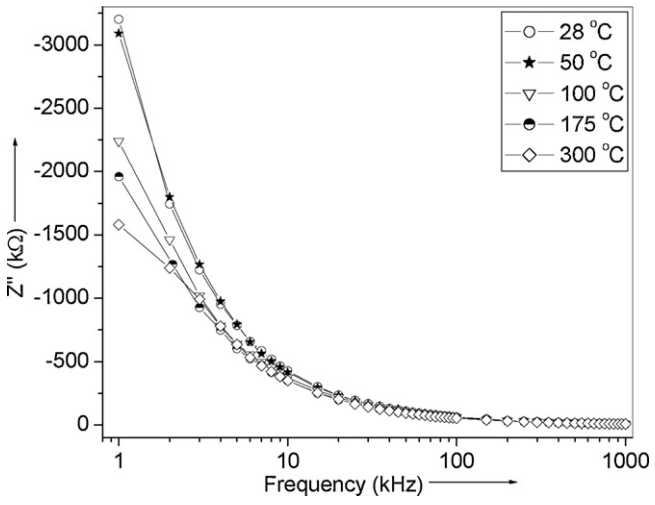

Fig. 6. Frequency dependence of Z'' at different temperatures.

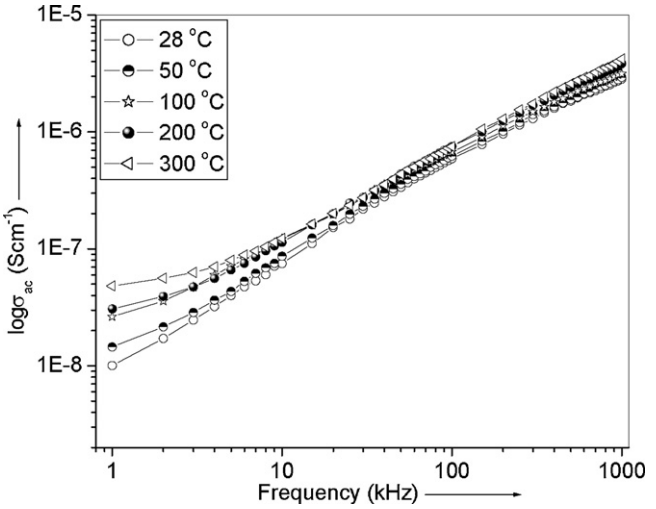

Fig. 7. Frequency dependence of σ_{ac} at different temperatures.

side. This merger of curves at high frequency side is due to the depletion of space charges [33,34].

Fig. 7 gives frequency dependence of a.c. conductivity (σ_{ac}) at different temperatures. It is seen from Fig. 7 that σ_{ac} decreases with decrease in frequency and becomes independent of frequency after a certain value. This value is known as hopping frequency, which shifts towards the high frequency side on increasing the temperature. The part below the hopping frequency is corresponding to the σ_{dc}. These features suggest that the mechanism of electrical conduction in the material is a hopping type, which follows the Jonscher's power equation $[\sigma(\omega) = \sigma_{dc} + A(\omega)^n]$, where n is the frequency exponent in the range $0 \leq n \leq 1$ and A is a constant that depends upon temperature [29,35,36]. Furthermore, increasing nature of σ_{ac} with temperature suggests about electrical conduction in the material as a thermally activated process.

4. Conclusions

A solution-based chemical method was used to prepare $LiZnVO_4$. X-ray diffraction study reveals a rhombohedral unit cell structure of the compound. The field emission scanning electron micrograph shows a polycrystalline texture of the compound with grains of unequal sizes ~0.2–2.0 μm. Impedance plots show the non-Debye type behavior of the material and electrical conduction in the material due to the bulk effect. A detailed study of the conductivity indicates electrical conduction in the material as a thermally activated process.

Acknowledgement

The author is grateful to the Nanomaterials Laboratory of the Department of Chemistry and Central Research Facility, Indian Institute of Technology, Kharagpur-721302 (W.B.), India, for providing facilities to conduct experiments.

References

[1] F. Gang, C. Huan, H. Sumei, L. Zhiyu, Sens. Actuators B: Chem. 137 (2009) 17.
[2] Y.C. Si, L.F. Jiao, H.T. Yuan, H.X. Li, Y.M. Wang, J. Alloys Compd. 486 (2009) 400.
[3] L.H. Chi, N.N. Dinh, S. Brutti, B. Scrosati, Electrochim. Acta 55 (2010) 5110.
[4] M.V. Reddy, A. Levasseur, J. Electroanal. Chem. 639 (2010) 27.
[5] H. Demidzu, T. Nakamura, Y. Yamada, J. Magn. Magn. Mater. 322 (2010) 1816.
[6] M. Ram, J. Alloys Compd. 509 (2011) 1744.
[7] S. Hu, G. Fu, Sens. Actuators A: Phys. 163 (2010) 481.
[8] G.M. Koenig Jr., I Belharouak, H.M. Wu, K. Amine, Electrochim. Acta 56 (2011) 1426.
[9] D. Gao, Y. Li, X. Lai, J. Bi, D. Lin, J. Alloys Compd. 509 (2011) 697.

[10] J.R. MacDonald, Impedance Spectroscopy: Emphasizing Solid Materials and Systems, John Wiley & Sons, New York, 1987.
[11] I. Soibam, S. Phanjoubam, L. Radhapiyari, Physica B 405 (2010) 2181.
[12] P.P. Hankare, R.P. Patil, U.B. Sankpal, K.M. Garadkar, R. Sasikala, A.K. Tripathi, I.S. Mulla, J. Magn. Magn. Mater. 322 (2010) 2629.
[13] R. Hariharan, P. Gopalan, Solid State Sci. 13 (2011) 168.
[14] K.M. Batoo, Physica B 406 (2011) 382.
[15] K. Prasad, Priyanka, K.P. Chandra, A.R. Kulkarni, J. Non-Cryst. Solids 357 (2011) 1209.
[16] E. Kazakevicius, A. Urcinskas, A. Kezionis, A. Dindune, Z. Kanepe, J. Ronis, Electrochim. Acta 51 (2006) 6199.
[17] T. Fehr, E. Schmidbauer, Solid State Ionics 178 (2007) 35.
[18] S. Tangwancharoen, P. Thongbai, T. Yamwong, S. Maensiri, Mater. Chem. Phys. 115 (2009) 585.
[19] M. Ram, Curr. Appl. Phys. 10 (2010) 1013.
[20] M. Ram, Physica B 405 (2010) 2205.
[21] M. Ram, Solid State Sci. 12 (2010) 350.
[22] M. Ram, Physica B 405 (2010) 1706.
[23] M.E. Brown, Introduction to Thermal Analysis: Technique and Applications, Chapman and Hall, New York, 1988.
[24] K. Selvaraj, C. Theivarasu, Thermochim. Acta 401 (2003) 187.
[25] E. Wu, POWD MULT: An Interactive Powder Diffraction Data Interpretation and Indexing Program, Version 2.1, School of Physical Sciences, Flinder University of South Australia, Bardford Park, SA, Australia, 1989.
[26] K. Umakantham, K. Chandramouli, G.N. Rao, A. Bhanumati, Bull. Mater. Sci. 19 (1996) 345.
[27] U. Intatha, S. Eitssayeam, J. Wang, T. Tunkasiri, Curr. Appl. Phys. 10 (2010) 21.
[28] S. Kumar, K.B.R. Varma, Solid State Commun. 146 (2008) 137.
[29] D.K. Kanchan, K.P. Padmasree, H.R. Panchal, A.R. Kulkarni, Ceram. Int. 30 (2004) 1655.
[30] Y. Cui, L. Zhang, G. Xie, R. Wang, Solid State Commun. 138 (2006) 481.
[31] Y.M. Li, R.H. Liao, X.P. Jiang, Y.P. Zhang, J. Alloys Compd. 484 (2009) 961.
[32] Y.M. Li, W. Chen, J. Zhou, Q. Xu, X.Y. Gu, R.H. Liao, Physica B 365 (2005) 76.
[33] A.K. Jonscher, Dielectric Relaxation in Solids, Chelsca Dielectric Press, London, 1983.
[34] A.R. James, S. Balaji, S.B. Krupanidhi, Mater. Sci. Eng. B 64 (1999) 149.
[35] A.K. Jonscher, Nature 267 (1977) 673.
[36] K.P. Padmasree, D.K. Kanchan, Mater. Chem. Phys. 91 (2005) 551.